Fusion evaporation-residue cross sections for $^{28}Si+^{40}Ca$ at $E(^{28}Si)=309$, 397, and 452 MeV

M. F. Vineyard, J. S. Bauer,* J. F. Crum, C. H. Gosdin,† and R. S. Trotter‡
Department of Physics, University of Richmond, Richmond, Virginia 23173

D. G. Kovar,§ C. Beck,** D. J. Henderson, R. V. F. Janssens, and B. D. Wilkins††
Physics Division, Argonne National Laboratory, Argonne, Illinois 60439

C. F. Maguire
Department of Physics and Astronomy, Vanderbilt University, Nashville, Tennessee 37235

J. F. Mateja
Division of Educational Programs, Argonne National Laboratory, Argonne, Illinois 60439

F. W. Prosser
Department of Physics, University of Kansas, Lawrence, Kansas 66045

G. S. F. Stephans
Laboratory for Nuclear Science, Massachusetts Institute of Technology, Cambridge, Massachusetts 02139
(Received 23 December 1991)

Velocity distributions of mass-identified evaporation residues produced in the $^{28}Si+^{40}Ca$ reaction have been measured at bombarding energies of 309, 397, and 452 MeV using time-of-flight techniques. These distributions were used to identify evaporation residues and to separate the complete-fusion and incomplete-fusion components. Angular distributions and upper limits for the total evaporation-residue and complete-fusion evaporation-residue cross sections were extracted at all three bombarding energies. The complete-fusion evaporation-residue cross sections and the deduced critical angular momenta are compared with earlier measurements and the predictions of existing models. The ratios of the complete-fusion evaporation-residue cross section to the total evaporation-residue cross section, along with those measured for the $^{28}Si+^{12}C$ and $^{28}Si+^{28}Si$ systems at the same energies, support the entrance-channel mass-asymmetry dependence of the incomplete-fusion evaporation-residue process reported earlier.

PACS number(s): 25.70.Jj

I. INTRODUCTION

Time-of-flight (TOF) measurements of the velocity spectra of evaporation residues (ERs) produced in heavy-ion reactions have shown that at bombarding energies above 10 MeV/nucleon the velocity centroids are inconsistent, in many cases, with those expected for a complete-fusion (CF) reaction [1-6]. These results have been interpreted as evidence that some fraction of the ERs arise from a composite nucleus, formed in a pre-equilibrium or incomplete-fusion (ICF) process, which is moving at a velocity different from that of the CF compound nucleus. The behavior observed is qualitatively consistent with the picture that particle emission from the projectile and/or target occurs prior to fusion, where the emission from the lighter reaction partner is dominant. Also, certain systematics [5] appear to indicate that the incomplete-fusion evaporation-residue (ICFER) process depends on the mass asymmetry in the entrance channel.

In this paper, we present measurements of velocity distributions and fusion ER cross sections for ^{28}Si induced reactions on ^{40}Ca at bombarding energies of 309, 397, and 452 MeV (11, 14, and 16 MeV/nucleon, respectively). This is part of a systematic study of ^{28}Si induced reactions on ^{12}C [7], ^{28}Si [8], and ^{40}Ca targets to investigate the energy and target dependence of the ICFER process. The ratios of complete-fusion evaporation-residue (CFER) cross section to ER cross section reported here, along with those measured for the ^{12}C and ^{28}Si targets, support the mass-asymmetry dependence of the ICFER process.

*Present address: Air Products and Chemicals, Inc., Allentown, PA 18195-1501.
†Present address: Tulane University School of Medicine, New Orleans, LA 70118.
‡Present address: Department of Civil Engineering, University of Virginia, Charlottesville, VA 22901-2458.
§Present address: Division of Nuclear Physics, Department of Energy, Washington, D.C. 20585.
**Present address: Centre de Recherches Nucleaires, Strasbourg, France.
††Present address: Division of Environmental Assessments and Information Services, Argonne National Laboratory, Argonne, IL 60439.

The experimental procedure is described in Sec. II. In Sec. III the data analysis is discussed and the experimental results are presented. The results are discussed in the context of previous measurements and existing models in Sec. IV and a summary is presented in Sec. V.

II. EXPERIMENTAL PROCEDURE

The experiments were performed using pulsed ^{28}Si beams obtained from the Argonne National Laboratory ATLAS facility. These beams were incident on a self-supporting (370 μg/cm^2) ^{40}Ca target mounted in the ATLAS 91-cm scattering chamber. Mass identification of the reaction products was obtained with the use of two TOF detectors. The first TOF arm consisted of a gridless, carbon foil (20 μg/cm^2) microchannel plate (MCP) detector to provide the start signal and a $\Delta E-E$ Si telescope to obtain the stop signal (ΔE) and full energy ($\Delta E+E$) of each particle. The length of the flight path was 89.8 cm and the resolution of the time measurement was approximately 120 ps (FWHM). In the second TOF arm, a $\Delta E-E$ Si telescope was again used to obtain the stop (ΔE) and full energy ($\Delta E+E$) signals. However, mass identification was achieved using the rf beam timing of ATLAS. The length of the flight path was 65.6 cm and the time resolution of the ^{28}Si beam pulses was better than 150 ps. An example of the mass resolution attained is shown in Fig. 1. The ERs were stopped in the ΔE detectors (thickness 250 μm) at all three energies and the E detectors were used to measure the elastic scattering.

The beam direction was established to within 0.05° from measurements of the elastic scattering of ^{28}Si from a ^{197}Au target at small angles (3°–5°) on both sides of the beam. The relative angle between the two TOF arms and the solid angles of the detectors were established from elastic scattering of tandem-energy ^{28}Si (76.5 MeV) and ^{58}Ni (79 MeV) beams from the ^{197}Au target. Both the Faraday cup beam integrator and a monitor detector were used to establish the relative normalization between different runs. The two normalizations were found to be in good agreement. Absolute cross sections were determined by measuring the elastic scattering of 76.5 MeV ^{28}Si ions from the ^{40}Ca target at $\theta_{lab}=5°-30°$ and comparing with the Rutherford scattering predictions. The cross sections have been corrected for the efficiency of the MCP detector.

The energy and time calibrations of the detectors were derived from the elastic scattering of ^{28}Si and ^{58}Ni ions from the ^{197}Au target, along with the 5.486 MeV alpha group from an ^{241}Am source. Each measured fragment energy was corrected event by event for energy losses in the target, channel plate foil, gold layers on the front surface of the Si detectors, and aluminum layer on the back surface of the ΔE detector when applicable. Pulse-height-defect corrections based upon the method of Kaufman *et al.* [9] were made for each of the Si detectors. The scaling factor of the pulse-height-defect correction was determined for each Si detector from the pulse heights induced by the elastically scattered tandem-energy ^{28}Si and ^{58}Ni ions. Plasma delay corrections which affect the timing signal obtained from Si detectors

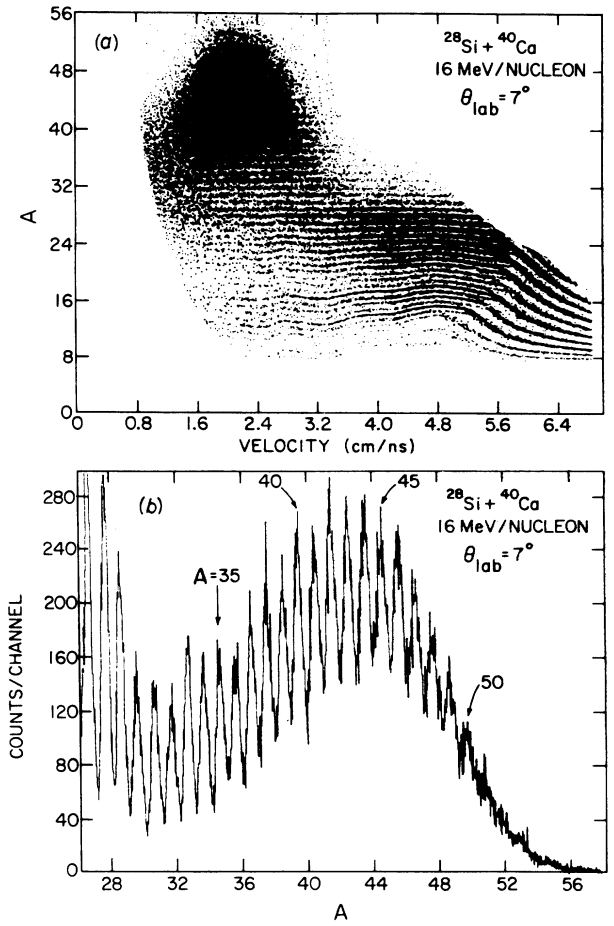

FIG. 1. (a) Two-dimensional mass vs velocity spectrum for ^{28}Si+^{40}Ca at E_{lab}=452 MeV (16 MeV/nucleon) and θ_{lab}=7°. (b) The corresponding mass spectrum. A software gate on the energy was used to exclude the elastic scattering from these spectra.

were also applied to the data following the prescription by Bohne *et al.* [10].

The velocities of the reaction products were extracted using two complimentary techniques: (1) by direct TOF measurement corrected for plasma delay, and (2) by using the measured energies corrected for pulse-height defect and energy losses along with the mass identification. The two sets of velocity spectra agreed to within 1.5% at the lowest bombarding energy. However, discrepancies as large as 3.5% were found for the heavier masses at the two higher bombarding energies. It was determined that this is due to the plasma delay correction. Since the pulse-height defect correction is much better understood, and has only one adjustable parameter which was experimentally determined for each of our detectors, the velocity spectra obtained from the measured energies were used in the analysis of the data. The uncertainty in the velocity measurement of the ERs is estimated to be ±0.025 cm/ns.

III. DATA ANALYSIS AND EXPERIMENTAL RESULTS

The velocity spectra of the reaction products were used to distinguish between ER yields and those arising from

binary reactions which populate some of the same mass groups. The origin of similar binary yields observed in slightly lighter systems has been discussed in terms of fusion-fission [11] and deep-inelastic processes [12,13] and it is possible that both mechanisms contribute. The velocity spectra were also used to extract information about the relative contributions of CF and ICF. In this section, we discuss how the ER yields were identified and how they were decomposed into CF and ICF contributions.

The difficulty in extracting the ER yields can be understood from a close inspection of Fig. 1. Shown in this figure is a two-dimensional mass versus velocity spectrum and a one-dimensional mass spectrum taken at a bombarding energy of 452 MeV and a laboratory angle of 7°. It is obvious that at this energy there is not a distinct separation between ERs and products from other reaction processes as is the case at low bombarding energy. For lower ER masses there is clear evidence of a reaction component which does not follow the average velocity of the center of mass. This can be seen in Fig. 2, where the Galilean-invariant velocity spectra $[(1/v^2)d^2\sigma/d\Omega\, dv]$ for masses 50 and 40 taken at a bombarding energy of 397 MeV and a laboratory angle of 5° are presented. The velocity distribution for $A=50$ is Gaussian and typical of what is observed for the heavier masses. The velocity spectrum for $A=40$, on the other hand, shows evidence of additional components.

To extract ER yields, the Galilean-invariant cross sections for the ERs are assumed to have a Gaussian shaped distribution, with a centroid shifted to lower velocity and with a broader width than expected for CF due to the contribution from ICF. This assumption is based on the behavior observed for the heavier ER masses, where there is little ambiguity in the identification, and on the results of calculations with the statistical model code PACE [14]. In studies involving asymmetric systems, the magnitude of the shift of the velocity centroid with respect to that expected for CF is understood to reflect the relative importance of ICF contributions. The shift is generally expressed in terms of the ratio

$$R_v = V_{\text{centroid}}/(V_{\text{c.m.}}\cos\theta_{\text{lab}}) ,$$

where $V_{\text{c.m.}}$ is the center-of-mass velocity of the system and θ_{lab} is the laboratory angle at which the centroid is observed. The velocity $V_{\text{c.m.}}\cos\theta_{\text{lab}}$ is the average velocity expected for ERs produced in a CF reaction assuming the evaporated light particles are emitted isotropically in the frame of the compound nucleus [15]. It has recently been shown [6] that anisotropic emission of the evaporated light particles produces small deviations from the simple $V_{\text{c.m.}}\cos\theta_{\text{lab}}$ behavior, but the shapes for all practical purposes remain Gaussian. The ratios R_v extracted from the 309 and 397 MeV data at $\theta_{\text{lab}}=5°$ and the 452 MeV data at $\theta_{\text{lab}}=7°$ are shown in Fig. 3 as a function of mass number. The solid horizontal lines are the results expected assuming isotropic emission of the evaporated light particles and the dashed curves are the results of a PACE calculation. The data show a shift in the velocity centroids which increases with bombarding energy and indicates significant ICF contributions at all three energies. The average ratios $\langle R_v \rangle$, obtained by averaging over mass and angle at each energy, are compared with previous measurements [16] in Table I. The widths (FWHM) of the velocity distributions at $E_{\text{lab}}=309$ MeV, plotted as a function of (a) mass at $\theta_{\text{lab}}=5°$ and (b) angle for mass 54, are shown in Fig. 4. The PACE calculation (solid curve) correctly predicts the trend of the mass and angle dependence of the widths. However, the magnitude of the widths is underpredicted indicating the presence of ICF processes. This discrepancy between the observed and predicted widths was found at all three bombarding energies and increased with bombarding energy.

The invariant ER cross sections were determined for each mass using a Gaussian shaped velocity distribution with a fixed centroid and a width allowed to vary smoothly with mass. The width for a given mass was fixed for all the measured angles. The centroid and mass dependence of the width was established by fitting the heavier masses. For the heavier masses, such as $A=50$ at $E_{\text{lab}}=397$ and $\theta_{\text{lab}}=5°$ whose velocity spectrum is shown in Fig. 2, this procedure was straightforward and yields were obtained with relatively small uncertainties. However, for the lighter masses, larger uncertainties are associated with this procedure. Due to the presence of binary-reaction components in the velocity spectra of these lighter masses, it is sometimes difficult to identify a Gaussian component and, even when a Gaussian component is apparent, it is difficult to estimate the "background" contributions. In these cases, the yields were extracted by adjusting the amplitude of the Gaussian to the maximum value consistent with the data. An example of this is

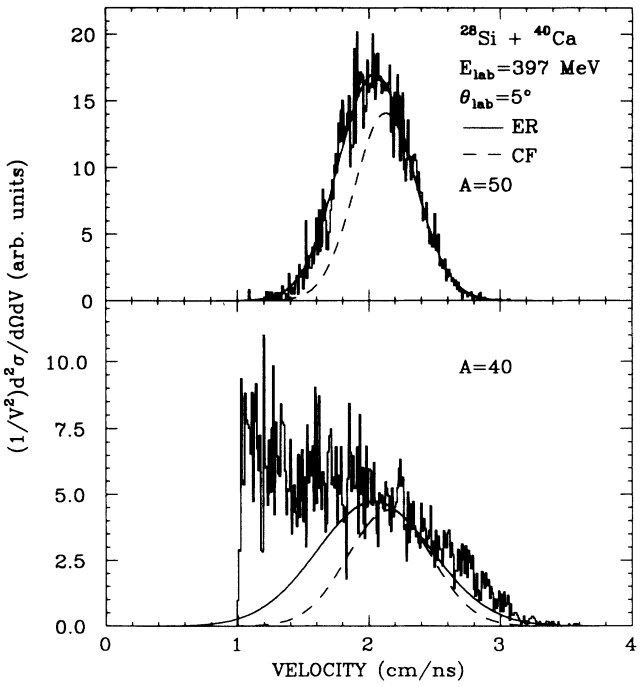

FIG. 2. The Galilean-invariant velocity spectra observed for masses 50 and 40 at $E_{\text{lab}}=397$ MeV and $\theta_{\text{lab}}=5°$. The curves are the Gaussian fits to the data as described in the text.

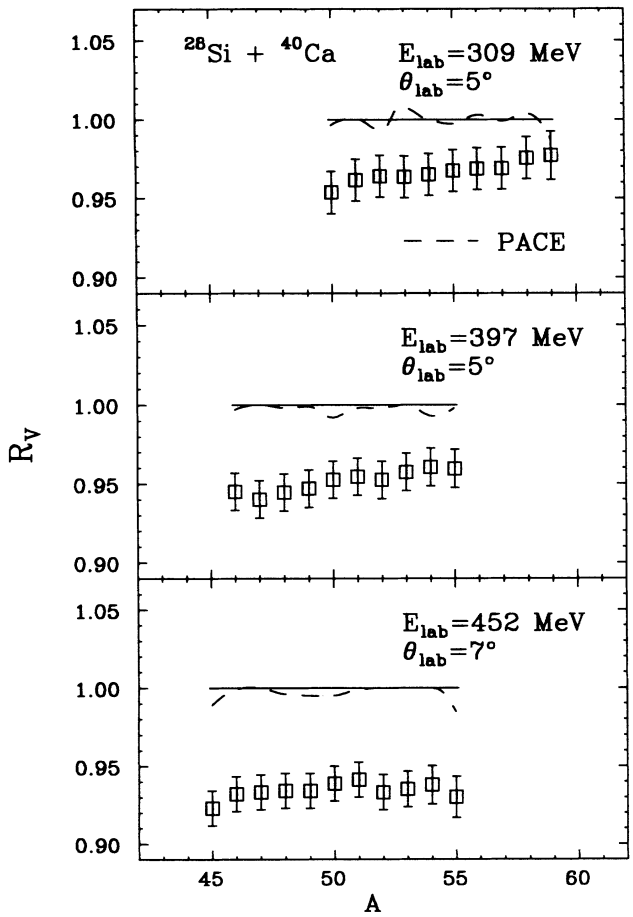

FIG. 3. The ratios $R_v = V_{centroid}/(V_{c.m.}\cos\theta_{lab})$ extracted from the data plotted as a function of mass number for a representative angle at each bombarding energy. The solid horizontal lines indicate the results expected assuming isotropic emission of the evaporated light particles and the dashed curves are the results of PACE calculations. Only the masses for which the yields appear to be of purely evaporation-residue origin are included in the figure.

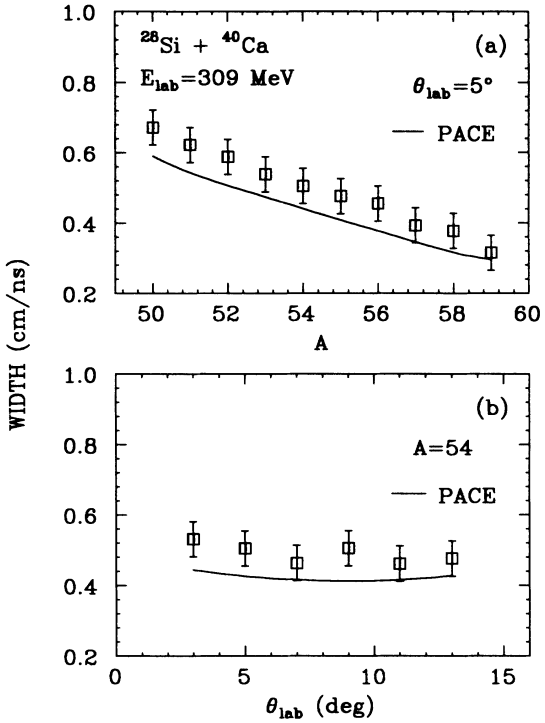

FIG. 4. The widths (FWHM) of the velocity distributions at $E_{lab}=309$ MeV plotted as a function of (a) mass at $\theta_{lab}=5°$ and (b) angle for mass 54. The solid lines represent the predictions of the code PACE. Only the masses for which the yields appear to be of purely evaporation-residue origin are included in the figure.

shown in Fig. 2 for $A=40$ at $E_{lab}=397$ MeV and $\theta_{lab}=5°$. These yields are considered to be maximum limits on the ER yields. It was not clear from the data how far down to lower masses this procedure should be carried. Therefore, we chose to include those masses that together correspond to 99% of the PACE predicted mass distribution. Statistical model calculations for ICF processes yield mass distributions which are only slightly shifted to lower masses indicating that this is a reasonable procedure. The angle-integrated ER mass distributions are shown in Fig. 5. In Fig. 6 the angular distributions of the total ER cross sections are presented.

Once the ER yields were identified they were decomposed into CF and ICF contributions. The CF component was determined by assuming a Gaussian velocity distribution with a centroid and width predicted by PACE and by normalizing the amplitude to the maximum value consistent with the data. This is illustrated in Fig. 2 for $A=50$ and 40 at $E_{lab}=397$ MeV and $\theta_{lab}=5°$. The shape of the velocity spectra were found to be consistent with the assumption that contributions to ICF corresponding to preequilibrium emission from the ^{40}Ca nucleus are negligible. The angle-integrated CFER mass distributions are compared to those of the ERs and the PACE predictions in Fig. 5. The summed angular distributions for the ER yields (squares) and the CFER yields (diamonds)

TABLE I. Experimental average velocity-deficit ratios and cross sections.

E_{lab} (MeV)	$\langle R_v \rangle$	σ_{ER} (mb)	σ_{CFER} (mb)	Ref.
298	0.960±0.013	923±106	646±100	[16]
309	0.964±0.009	855±128	631±126	Present work
327	0.955±0.009	898±143	548±130	[16]
397	0.939±0.018	712±107	519±104	Present work
452	0.931±0.008	600±90	379±76	Present work

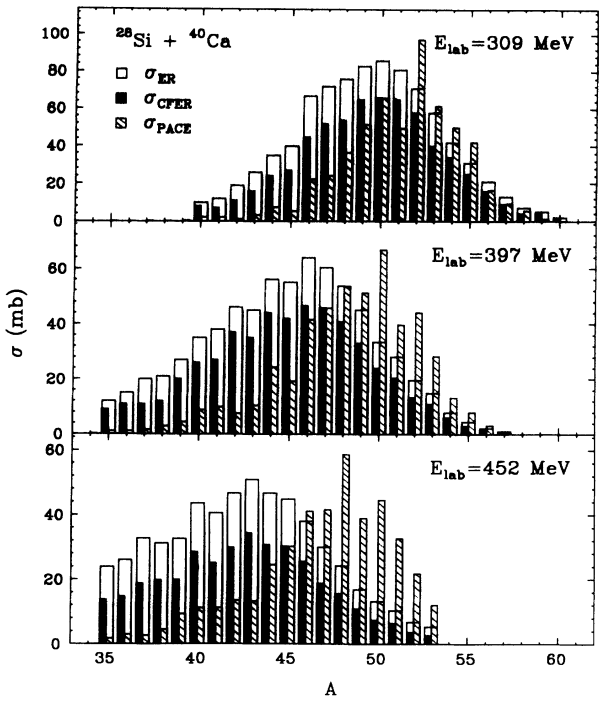

FIG. 5. Angle-integrated evaporation-residue (ER) and complete-fusion evaporation-residue (CFER) mass distributions compared with the PACE predictions.

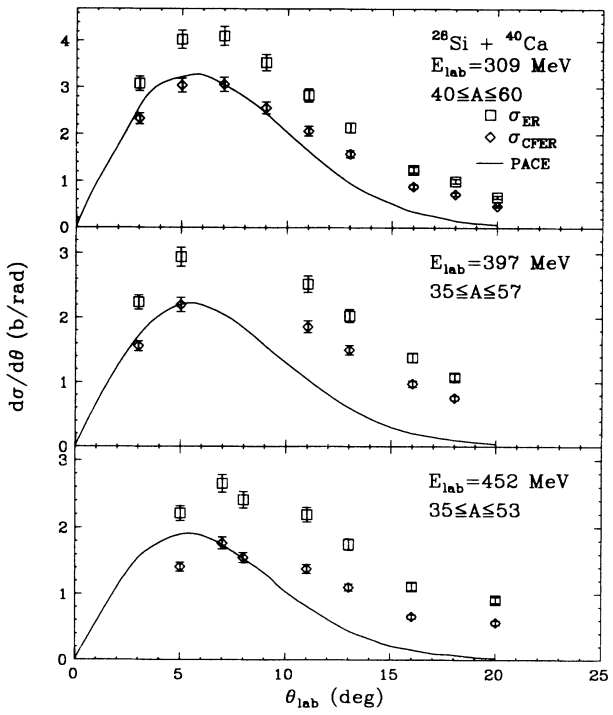

FIG. 6. The total evaporation-residue (squares) and complete-fusion evaporation-residue (diamonds) angular distributions resulting from the decomposition of the velocity spectra. The solid curves are PACE predictions normalized to the most forward angle data points.

obtained using the procedures described above are presented in Fig. 6.

The total ER cross sections and the total CFER cross sections, found by integrating the angular distributions (using a smooth extrapolation at the two angular extremes), are compared with earlier measurements [16] in Table I. These cross sections must be considered as upper limits. The uncertainty in the absolute ER cross sections arise from counting statistics, uncertainties in the absolute normalization, extrapolations beyond the measured angular ranges, and the procedure used to extract the yields for the lighter masses. The errors associated with the CFER cross sections also include estimates of the uncertainties due to the fitting procedure.

IV. DISCUSSION

The solid curves in Fig. 6 are the CFER angular distributions predicted by PACE and normalized to the data at forward angles. As can be seen, the measured angular distributions are broader than the predictions. A disagreement between the data and the predictions of CF evaporation calculations also exists in the mass distributions shown in Fig. 5. The PACE predicted mass distribution is shifted to larger mass with respect to the extracted CF mass distribution. These discrepancies have been observed in earlier studies [6,8] and have been interpreted as evidence of heavy particle evaporation. However, it should be noted that the possibility cannot be ruled out that the effects observed here may be due, at least in part, to misidentification of the yields at larger angles for the lighter masses.

The total CFER cross sections measured in the present study are plotted along with the previous measurements of Pochodzalla *et al.* [16] in Fig. 7. The two sets of data are in rather good agreement (see Table I). The solid curve shown in the figure is the prediction of the critical distance [17] fusion model. The dashed curve is the result of a calculation for the ^{32}S+^{40}Ca system using the surface friction [18] model. The experimental cross sections in this energy region are overpredicted by both of these models. This discrepancy has been observed in earlier studies [6,8] and it has been suggested that it may reflect the fact that fission channels are implicitly included in the model calculations, but not in the data. The total fission cross section behavior for ^{28}Si+^{40}Ca has not been established. However, recent studies [6,19,20] of systems forming the ^{56}Ni compound nucleus have indicated the presence of substantial fission cross sections, and, therefore, one might expect a significant fusion-fission contribution in the ^{28}Si+^{40}Ca reaction.

The critical angular momenta extracted from the experimental CFER cross sections using the sharp cutoff approximation are plotted versus the excitation energy of the ^{68}Se compound nucleus in Fig. 8. The solid vertical line in the figure indicates the angular momentum at which the calculated fission barrier of ^{68}Se vanishes. This calculation was performed with the Sierk [21] model. The comparison of these extracted critical angular momenta with the calculated fission-barrier limit indicates that the CFER process is limited by fission competition

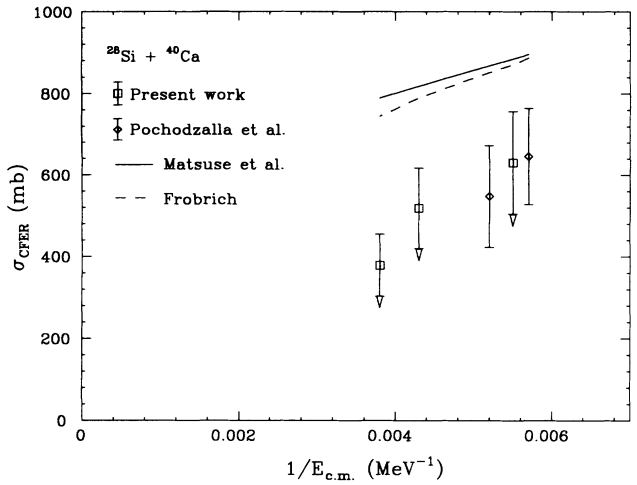

FIG. 7. Complete-fusion evaporation-residue cross sections for the ^{28}Si+^{40}Ca reaction. The data points are from Ref. [16] (diamonds) and the present work (squares). The solid curve is the prediction of the critical distance fusion model of Ref. [17]. The dashed curve is the result of a fusion model calculation for the ^{32}S+^{40}Ca system taken from Ref. [18].

at these high energies as suggested earlier [16].

In an earlier study, Morgenstern *et al.* [5] extracted the ratios of CFER to total ER cross sections for systems with differing mass asymmetry in the entrance channel. Their results indicate that the CFER process is more likely for an asymmetric system than for a symmetric system at the same relative velocity. A common onset of the ICFER process for systems with different mass asymmetry in the entrance channel was found only when the data were plotted as a function of the center-of-mass velocity of the lighter reaction partner at contact; i.e.,

$$v_L = [A_H/(A_H + A_L)]v_{\rm rel} ,$$

where A_H and A_L are the masses of the heavier and lighter reaction partner, respectively. The relative velocity, $v_{\rm rel}$, is defined as

$$v_{\rm rel} = [2(E_{\rm c.m.} - V_C)/\mu]^{1/2} ,$$

where $E_{\rm c.m.}$ and V_C are the center-of-mass kinetic and Coulomb energies, respectively, and μ is the reduced mass. The trends of the Morgenstern results are shown as the solid curves in Fig. 9. The asymmetric systems fell primarily along the upper curve, while the symmetric systems clustered around the lower curve. Also shown in the figure are the data from the present work and earlier studies of ^{28}Si induced reactions with ^{12}C [7], ^{28}Si [8], and ^{40}Ca [16]. The ^{28}Si+^{12}C and ^{28}Si+^{28}Si measurements were performed at the same bombarding energy as the ^{28}Si+^{40}Ca measurements reported in this study and the data were analyzed in a consistent fashion. Within the errors, these data agree with the Morgenstern systematics and substantiate the entrance-channel mass-asymmetry dependence of the ICFER process.

The shifts of the velocity distributions observed in this study are consistent with those reported previously for ^{28}Si+^{40}Ca at $E(^{28}\text{Si}) = 298$ and 327 MeV [16]. The number of preequilibrium nucleons responsible for the missing momentum can be estimated [3,6] under the assumption that they are emitted along the beam axis with the velocity of the projectile and is found to be 1.9±0.5, 1.7±0.4, 2.1±0.4, 2.8±0.8 and 3.1±0.4 at 298, 309, 327, 397, and 452 MeV, respectively. These numbers are

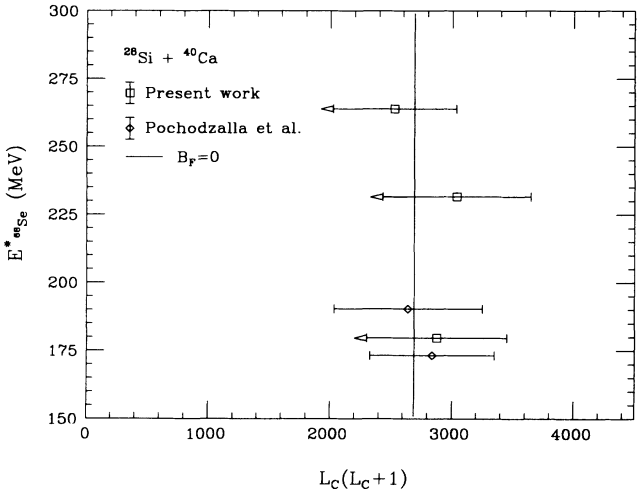

FIG. 8. Compound nucleus excitation energy vs the product $L_c(L_c+1)$, where L_c is the critical angular momentum extracted from the complete-fusion evaporation-residue cross sections of Ref. [16] (diamonds) and the present work (squares). The solid vertical line indicates the predicted angular momentum at which the fission barrier vanishes using the model of Sierk [21].

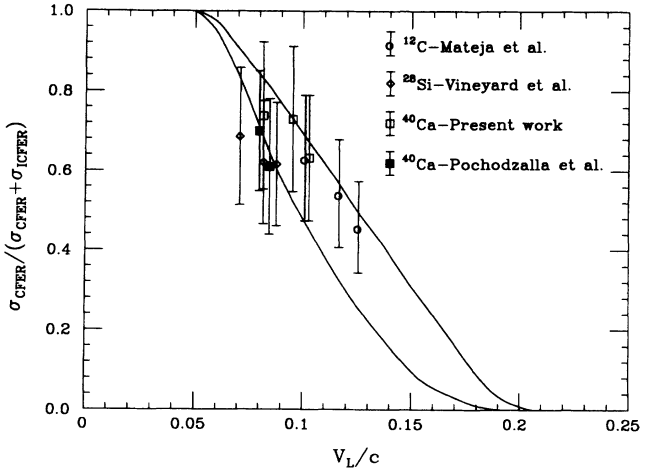

FIG. 9. The ratio of complete-fusion evaporation-residue cross section to total evaporation-residue cross section as a function of the velocity of the lighter nucleus V_L/c. The data for the ^{12}C and ^{28}Si targets are from Refs. [7,8], respectively. The data for the ^{40}Ca target are from Ref. [16] and the present work. The curves represent the trends from Ref. [5]. In that study, it was found that the mass-asymmetric systems fell primarily along the upper curve, while the symmetric systems clustered around the lower.

in agreement with the systematics of Stephans *et al.* [3] which show that the number of emitted nucleons necessary to explain the observed velocity centroids depends strongly on the projectile.

V. SUMMARY

Evaporation-residue-like fragments produced by bombarding a ^{40}Ca target with ^{28}Si at laboratory energies of 309, 397, and 452 MeV have been studied using pulsed beams obtained from the ATLAS facility. Time-of-flight techniques enabled the extraction of the velocity distributions of the resolved ER mass groups. The shifts in the centroids of these distributions, compared with those expected for complete momentum transfer, indicate the presence of significant ICF processes at all three energies. The velocity spectra were used to separate the CF and ICF components with the aid of evaporation-code calculations. Complete angular distributions for ERs and for yields consistent with CF were obtained at all three energies.

The measured CFER angular distributions are broader than evaporation-code predictions. Also, the predicted mass distributions are shifted to higher mass than the experimental distributions. Similar observations have been made in earlier studies and are interpreted as evidence for the presence of heavy particle evaporation or very mass-asymmetric fission.

The upper limits for the total ER and CFER cross sections obtained in this study are consistent with those measured previously for the ^{28}Si+^{40}Ca system at $E(^{28}\text{Si})=298$ and 327 MeV. The CFER cross sections at these energies are overpredicted by fusion models and appear to be limited by fission competition. Additional experiments are needed to establish the fusion-fission cross section and understand the limitations on the CF process.

The ratios of CFER to total ER cross sections and the shifts of the velocity distributions obtained in this study are consistent with earlier measurements and previously established systematic which argue for an entrance-channel mass-asymmetry dependence of the ICFER process. We have now completed a consistent analysis of ERs produced by bombarding ^{12}C, ^{28}Si, and ^{40}Ca targets with ^{28}Si at three energies, and have verified this behavior within the errors of the measurements. Coincidence measurements are needed to investigate the importance of ICF in the fission exit channels for systems with different mass asymmetry in the entrance channel.

ACKNOWLEDGMENTS

This work was supported by the U.S. Department of Energy, Nuclear Physics Division, under Contracts No. W-31-109-Eng-38, DE-FG05-88ER40459, DE-AC02-79ER10420, and DE-FG02-89ER40506. Four of the authors (M.F.V., J.S.B., C.F.M., and F.W.P.) also wish to acknowledge the financial support of Argonne National Laboratory.

[1] H. Morgenstern, W. Bohne, K. Garbisch, D. G. Kovar, and H. Lehr, Phys. Lett. **113B**, 463 (1982); H. Morgenstern, W. Bohne, K. Garbisch, H. Lehr, and W. Stoffler, Z. Phys. A **313**, 39 (1983).

[2] G. Rosner, J. Pochodzalla, B. Heck, G. Hlawatsch, A. Miczaika, J. H. Rabe, R. Butsch, B. Kolb, and B. Sedelmeyer, Phys. Lett. **150B**, 87 (1985).

[3] G. S. F. Stephans, D. G. Kovar, R. V. F. Janssens, G. Rosner, H. Ikezoe, B. Wilkins, D. Henderson, K. T. Lesko, J. J. Kolata, C. K. Gelbke, B. V. Jacak, Z. M. Koenig, G. D. Westfall, A. Szanto De Toledo, E. M. Szanto, and P. L. Gonthier, Phys. Lett. **161B**, 60 (1985).

[4] Y. Chan, M. Murphy, R. G. Stokstad, I. Tserruya, S. Wald, and A. Budzanowski, Phys. Rev. C **27**, 447 (1983).

[5] H. Morgenstern, W. Bohne, W. Galster, K. Grabisch, and A. Kyanowski, Phys. Rev. Lett. **52**, 1104 (1984).

[6] C. Beck, D. G. Kovar, S. J. Sanders, B. D. Wilkins, D. J. Henderson, R. V. F. Janssens, W. C. Ma, M. F. Vineyard, T. F. Wang, C. F. Maguire, F. W. Prosser, and G. Rosner, Phys. Rev. C **39**, 2202 (1989).

[7] J. F. Mateja, M. F. Vineyard, S. J. Padalino, L. C. Dennis, A. D. Frawley, K. W. Kemper, M. Tiede, R. A. Zingarelli, D. G. Kovar, C. Beck, D. J. Henderson, R. V. F. Janssens, B. D. Wilkins, C. F. Maguire, F. W. Prosser, and G. F. S. Stephans (unpublished).

[8] M. F. Vineyard, J. S. Bauer, C. H. Gosdin, R. S. Trotter, D. G. Kovar, C. Beck, D. J. Henderson, R. V. F. Janssens, B. D. Wilkins, G. Rosner, P. Chowdhury, H. Ikezoe, W. Kuhn, J. J. Kolata, J. D. Hinnefeld, C. F. Maguire, J. F. Mateja, F. W. Prosser, and G. S. F. Stephans, Phys. Rev. C **41**, 1005 (1990).

[9] S. B. Kaufman, E. P. Steinberg, D. B. Wilkins, J. Unik, A. J. Gorski, and M. J. Fluss, Nucl. Instrum. Methods **115**, 47 (1974).

[10] W. Bohne, W. Galster, K. Grabisch, and H. Morgenstern, Nucl. Instrum. Methods **A240**, 145 (1985).

[11] S. J. Sanders, D. G. Kovar, B. B. Back, C. Beck, D. J. Henderson, R. V. F. Janssens, T. F. Wang, and B. D. Wilkins, Phys. Rev. C **40**, 2091 (1989), and references therein.

[12] D. Shapira, Phys. Rev. Lett. **61**, 2153 (1988), and references therein.

[13] W. Dunnweber, A. Glaesner, W. Hering, D. Konnerth, R. Ritzka, W. Trombik, J. Czakanski, and W. Zipper, Phys. Rev. Lett. **61**, 927 (1988).

[14] PACE is the modification of the code JULIAN described by A. Gavron, Phys. Rev. C **21**, 230 (1980).

[15] J. Gomez del Campo, R. G. Stokstad, J. A. Biggerstaff, R. A. Dayras, A. H. Snell, and P. H. Stelson, Phys. Rev. C **19**, 2170 (1979).

[16] J. Pochodzalla, R. Butsch, B. Heck, and G. Rosner, Phys. Lett. B **181**, 33 (1986).

[17] T. Matsuse, A. Arima, and S. M. Lee, Phys. Rev. C **26**, 2338 (1982).

[18] P. Frobrich, Phys. Rep. **116**, 337 (1984).

[19] S. J. Sanders, R. R. Betts, I. Ahmad, K. T. Lesko, S. Saini, B. D. Wilkins, F. Videbaek, and B. K. Dichter, Phys. Rev. C **34**, 1746 (1986).

[20] S. J. Sanders, D. G. Kovar, B. B. Back, C. Beck, B. K. Dichter, D. J. Henderson, R. V. F. Janssens, J. G. Keller, S. Kaufman, T. F. Wang, B. D. Wilkins, and F. Videbaek, Phys. Rev. Lett. **59**, 2856 (1987).

[21] A. J. Sierk, Phys. Rev. Lett. **55**, 582 (1985); Phys. Rev. C **33**, 2039 (1986).